

# Exciton swapping in a twisted graphene bilayer as a solid-state realization of a two-brane model

Michaël Sarrazin<sup>1,a</sup> and Fabrice Petit<sup>2</sup>

<sup>1</sup> Research Center in Physics of Matter and Radiation, University of Namur, 61 rue de Bruxelles, 5000 Namur, Belgium

<sup>2</sup> BCRC (Member of EMRA), 4 avenue du gouverneur Cornez, 7000 Mons, Belgium

Received 15 May 2013 / Received in final form 24 September 2013

Published online (Inserted Later) – © EDP Sciences, Società Italiana di Fisica, Springer-Verlag 2014

**Abstract.** It is shown that exciton swapping between two graphene sheets may occur under specific conditions. A magnetically tunable optical filter is described to demonstrate this new effect. Mathematically, it is shown that two turbostratic graphene layers can be described as a “noncommutative” two-sheeted  $(2 + 1)$ -spacetime thanks to a formalism previously introduced for the study of braneworlds in high energy physics. The Hamiltonian of the model contains a coupling term connecting the two layers which is similar to the coupling existing between two braneworlds at a quantum level. In the present case, this term is related to a  $K$ - $K'$  intervalley coupling. In addition, the experimental observation of this effect could be a way to assess the relevance of some theoretical concepts of the braneworld hypothesis.

## 1 Introduction

During the last few years, graphene has taken a growing importance in solid-state physics [1–41]. Indeed, it is an amazing case of two-dimensional carbon crystal, and its remarkable properties make it a strategic material for future nanotechnologies. For instance, doped graphene [36,37] thanks to electrostatic gating [38,39] can lead to efficient tunable optical devices. Moreover, recent works on graphene also underline the importance of electronic transport in turbostratic (twisted) bilayers [3–17]. In this context, the study of the specific features of graphene is of prime importance to develop new technological applications. In the present paper, we describe a new effect in which exciton swapping may occur between two graphene layers. An experimental device relying on a magnetically tunable optical filter is suggested. On a theoretical point of view, exciton swapping is well described by using a formalism introduced previously in high energy physics to describe the quantum dynamics of particles in a two-brane Universe.

During the last two decades, the possibility that our observable  $(3 + 1)$ -dimensional Universe could be a sheet (a 3-brane or braneworld) embedded in a  $(N + 1)$ -dimensional spacetime (called the bulk, with  $N > 3$ ) has received a lot of attention [42–45]. Such an exotic concept appears very productive to solve puzzling problems beyond the standard model of particles [42–45]. In recent papers [46–49], it was proved that in a universe made of two branes, the quantum dynamics of Dirac fermions can be rigorously described in a more simple

and equivalent frame that corresponds to a two-sheeted spacetime in the formalism of the noncommutative geometry [46,47]. Noncommutative geometry is a wide concept which covers different aspects [50–56]. For instance, it can concern a 3-dimensional space with noncommutative coordinates [40,41,54–56]. But it can also be a way to describe a discrete two-sheeted spacetime such that local coordinates (i.e. on each spacetime sheet) remain commutative [46,47,50–53]. In the braneworld model, the coupling term connecting the branes at a quantum level leads to Rabi oscillations between the two worlds, for particles endowed with a magnetic moment and subjected to a magnetic vector potential [46–49].

Graphene layers are known to be solid-state realizations of a  $(2 + 1)$ -spacetimes in which massless fermion live. For that reason, graphene is well adapted to study theoretically and experimentally concepts of low-dimensional electrodynamics and quantum dynamics [20–24]. Since a graphene sheet can be considered as 2-brane embedded in a  $(3 + 1)$ -bulk, a graphene bilayer could be a solid-state realization of a universe containing two branes (a two-brane universe). In the present paper, we show that this analogy is well-sounded and we demonstrate the possibility to apply tools from noncommutative geometry to study such a system. The fact that a noncommutative geometry can emerge in graphene is an intriguing possibility. Noncommutative geometry as a suitable tool to study graphene monolayer properties has already been reported in literature [40,41] in the context of noncommutative coordinates. Nevertheless, it will be shown in the present paper that a graphene bilayer can be a solid-state realization of a “noncommutative” two-sheeted spacetime.

<sup>a</sup> e-mail: michael.sarrazin@unamur.be

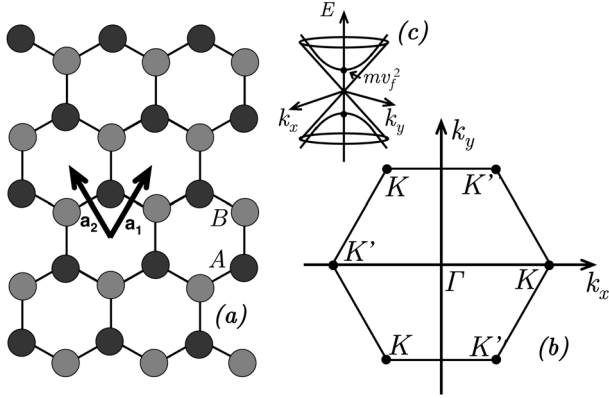


**Fig. 1.** (a) Hexagonal lattice of graphene with the two sublattices  $A$  and  $B$ .  $a_1$  and  $a_2$  are the vectors of the unit cell. (b) Brillouin zone of the hexagonal lattice. (c) Energy behavior in the vicinity of the Dirac points  $K$  and  $K'$ .

In addition, our approach suggests that exciton swapping may occur between the two graphene layers, which is a solid-state counterpart of particle oscillations predicted in brane theory [46–49].

In Section 2, we recall the basic assumptions underlying the description of electron and hole in graphene through a Dirac equation formalism. Next, in Section 3, we present the model of fermion dynamics in a two-sheeted spacetime and its adaptation to describe a set of two graphene layers. In Section 4, using a tight-binding approach, it is shown that considering two twisted graphene layers is a prerequisite to get a  $K$ - $K'$  intervalley coupling between two perfect graphene layers in mutual interaction as described in Section 3. This is this coupling which leads to excitonic swapping between the layers as shown in Section 5. Finally, in Section 6, an experimental device is suggested to investigate this new effect.

## 2 Graphene electronic properties

Graphene is a one-atom thick layer made of  $sp^2$  carbon atoms in an hexagonal lattice arrangement (Fig. 1a) [1,2]. Self-supported ideal graphene is a zero-gap semiconductor. In the vicinity of the six corners (called Dirac points) of the two-dimensional hexagonal Brillouin zone (Fig. 1b), the electronic dispersion relation is linear for low energies (Fig. 1c). Electrons (and holes) can then be described by a Dirac equation for massless spin-1/2 particles in an effective  $(2+1)$ -spacetime [2]. While massless Dirac fermions propagate at the speed of light in the  $(3+1)$  Minkowski spacetime, in graphene the effective massless Dirac fermions propagates at the Fermi velocity ( $v_F \approx 10^6$  m s $^{-1}$  in the present case). On a graphene layer, the Hamiltonian of the effective Dirac equation is given by [2]:

$$H_{\pm} = -i\hbar v_F(\sigma_1 \partial_x \pm \sigma_2 \partial_y) + m v_F^2 \sigma_3 \quad (1)$$

where “+” (respectively “-”) refers to the  $K$  (respectively  $K'$ ) Dirac point of the Brillouin zone of the graphene hexagonal structure (Fig. 1a).  $\sigma_k$  ( $k = 1, 2, 3$ ) are the usual

Pauli matrices. For a self-supported graphene sheet the mass term  $m$  is equal to zero and electrons (and holes) behave as relativistic quasiparticles. Nevertheless  $m$  may differ from zero in the case of a sheet deposited on a substrate [25–28]. Using  $m \rightarrow m v_F / \hbar$  and  $(x_0, x_1, x_2) = (v_F t, x, y)$ , from equation (1) it is possible to conveniently describe the electron (or hole) dynamics through an effective Dirac equation such that [2]:

$$(i\gamma^\eta \partial_\eta - m)\psi = 0 \quad (2)$$

with  $\eta = 0, 1, 2$  and

$$\gamma^0 = \begin{pmatrix} \sigma_3 & 0 \\ 0 & \sigma_3 \end{pmatrix}, \quad \gamma^1 = \begin{pmatrix} i\sigma_2 & 0 \\ 0 & i\sigma_2 \end{pmatrix}, \quad \gamma^2 = \begin{pmatrix} -i\sigma_1 & 0 \\ 0 & i\sigma_1 \end{pmatrix} \quad (3)$$

such that

$$\{\gamma^\eta, \gamma^\vartheta\} = 2g^{\eta\vartheta} \quad (\eta, \vartheta = 0, 1, 2)$$

with

$$g^{\eta\vartheta} = \text{diag}(1, -1, -1).$$

The wave function is defined as:

$$\psi = \begin{pmatrix} \chi \\ \theta \end{pmatrix}$$

where  $\chi$  (respectively  $\theta$ ) is related to the wave function on  $K$  (respectively  $K'$ ). In addition,  $\chi$  (respectively  $\theta$ ) can be written as:

$$\chi = \begin{pmatrix} \chi_A \\ \chi_B \end{pmatrix} \quad \left( \text{respectively} \quad \theta = \begin{pmatrix} \theta_A \\ \theta_B \end{pmatrix} \right)$$

where  $A$  and  $B$  are related to the two sublattices of the graphene sheet (see Fig. 1a). While one does not consider the usual electronic spin, a pseudospin arises, for which the two states are related to the two labels  $A$  and  $B$  of the graphene sublattices [1]. In addition, since there is two inequivalent families of Dirac cones (respectively located at points  $K$  and  $K'$  in the Brillouin zone), an isospin degree of freedom also arises from the two states associated with the two kinds of Dirac points [19].

It can be noticed that the above  $(2+1)$ -Dirac equation can be easily extended to its  $(3+1)$ -dimensional version.  $\gamma^3$  and  $\gamma^5$  matrices (such as  $\gamma^5 = i\gamma^0\gamma^1\gamma^2\gamma^3$ ) can be introduced and we may consider for instance:

$$\gamma^3 = \begin{pmatrix} 0 & -\sigma_1 \\ \sigma_1 & 0 \end{pmatrix}, \quad -i\gamma^5 = \begin{pmatrix} 0 & i\sigma_1 \\ i\sigma_1 & 0 \end{pmatrix}. \quad (4)$$

The Clifford algebra is verified since:

$$\{\gamma^\mu, \gamma^\nu\} = 2g^{\mu\nu}, \quad \{\gamma^5, \gamma^\nu\} = 0 \quad \text{and} \quad (-i\gamma^5)^2 = -1,$$

where  $g^{\mu\nu}$  is the four-dimensional metric tensor of the Minkowski spacetime (with  $\mu, \nu = 0, 1, 2, 3$ ). Note that the  $\gamma^3$  and  $\gamma^5$  matrices are interchangeable through substitutions  $\gamma^3 \rightarrow i\gamma^5$  and  $-i\gamma^5 \rightarrow \gamma^3$  which lead to equivalent descriptions. Moreover, it is well known that  $\gamma^5$  can be also used to define a five-dimensional Dirac equation as shown in Section 3.

### 3 Two-layer graphene as a “noncommutative” two-sheeted spacetime

Let us consider a graphene layer as a 3-brane, i.e. a three-dimensional space sheet, for which one dimension (say  $x_3$ ) is reduced to zero. We suggest to derive the graphene bilayer system description from the two-sheeted spacetime model introduced in previous works [46–49] by making  $x_3 \rightarrow 0$ . The resulting model will be supported in Section 4 with a tight-binding approach.

In a prior work, the relevance of the two-sheeted approach was rigorously demonstrated for braneworlds described by domain walls [46]. Indeed, when one studies the low-energy dynamics of a spin-1/2 particle in a two-brane Universe, the quantum dynamics of this particle is equivalent to the behavior it would have in a two-sheeted spacetime described by noncommutative geometry [46].

Specifically, a two-sheeted spacetime corresponds to the product of a four-dimensional continuous manifold with a discrete two-point space and can be seen as a five-dimensional universe with a fifth dimension reduced to two points with coordinates  $\pm\delta/2$ . Both sheets are separated by a phenomenological distance  $\delta$ , which is not the real distance between the graphene layers as shown in the next section. Mathematically, the model relies on a bi-euclidean space  $X = M_4 \times Z_2$  in which any smooth function belongs to the algebra  $A = C^\infty(M) \oplus C^\infty(M)$  and can be adequately represented by a  $2 \times 2$  diagonal matrix  $F = \text{diag}(f_1, f_2)$ . In the noncommutative geometry formalism, the expression of the exterior derivative  $D = d + Q$ , where  $d$  acts on  $M_4$  and  $Q$  on the  $Z_2$  internal variable, has been given by Connes and Lott [50,51]:  $D : (f_1, f_2) \rightarrow (df_1, df_2, g(f_2 - f_1), g(f_1 - f_2))$  with  $g = 1/\delta$ . Viet and Wali [52,53] have proposed a representation of  $D$  acting as a derivative operator and fulfilling the above requirements. Due to the specific geometrical structure of the bulk, this operator is given by:

$$D_\mu = \begin{pmatrix} \partial_\mu & 0 \\ 0 & \partial_\mu \end{pmatrix}, \quad \mu = 0, 1, 2, 3 \quad \text{and} \quad D_5 = \begin{pmatrix} 0 & g \\ -g & 0 \end{pmatrix}, \quad (5)$$

where the term  $g$  acts as a finite difference operator along the discrete dimension. Using (5), one can build the Dirac operator defined as  $\mathcal{D} = \Gamma^N D_N = \Gamma^\mu D_\mu + \Gamma^5 D_5$ . It is then convenient to consider the following extension of the gamma matrices (by using the Hilbert space of spinors [50,51]):

$$\Gamma^\mu = \begin{pmatrix} \gamma^\mu & 0 \\ 0 & \gamma^\mu \end{pmatrix} \quad \text{and} \quad \Gamma^5 = \begin{pmatrix} \gamma^5 & 0 \\ 0 & -\gamma^5 \end{pmatrix}. \quad (6)$$

In the present work,  $\gamma^\mu$  and  $\gamma^5 = i\gamma^0\gamma^1\gamma^2\gamma^3$  are the Dirac matrices defined by relations (3) and (4) relevant for graphene. We can therefore introduce a mass term  $M = m\mathbf{1}_{8 \times 8}$  as in the standard Dirac equation. The two-sheeted Dirac equation then writes [46–48]:

$$\begin{aligned} \mathcal{D}_{dirac} \Psi &= (i\mathcal{D} - M) \Psi = (i\Gamma^N D_N - M) \Psi \\ &= \begin{pmatrix} i\gamma^\mu \partial_\mu - m & ig\gamma^5 \\ ig\gamma^5 & i\gamma^\mu \partial_\mu - m \end{pmatrix} \begin{pmatrix} \psi_\alpha \\ \psi_\beta \end{pmatrix} = 0 \end{aligned} \quad (7)$$

with  $\Psi = \begin{pmatrix} \psi_\alpha \\ \psi_\beta \end{pmatrix}$  the two-sheeted wave function. In this notation, the indices “ $\alpha$ ” and “ $\beta$ ” discriminate each sheet [46–48], i.e. each graphene layer when  $x_3 \rightarrow 0$ . Each component of the wave function  $\psi$  is then the probability amplitude of the electron (or hole) in each graphene sheet. It is important to point out the Lagrangian term:

$$\mathcal{L}_c = \bar{\Psi} i\Gamma^5 D_5 \Psi \quad (8)$$

which ensures the coupling between each graphene layer through  $K$ - $K'$  processes as explained in Section 4. That means that the Lagrangian  $\mathcal{L}_c$  couples both each graphene layer but also the isospin states (thanks to the  $\gamma^5$  matrix). Conversely, in the present work the noncommutative geometry model emerges from  $K$ - $K'$  interlayer couplings. The  $\mathcal{L}_c$  term is the main reason for this paper as it will allow excitonic swapping between the graphene layers.

Let us now introduce the effect of an electromagnetic field, i.e. an  $U(1)$  gauge field. To be consistent with the two-sheeted structure of the Dirac field  $\Psi$  in equation (7), the usual  $U(1)$  electromagnetic gauge field should be replaced by an extended  $U(1) \otimes U(1)$  gauge field [46–48]. Nevertheless, in the present work, we assume that electromagnetic field sources are out of the graphene layers. The group representation  $G = \text{diag}(\exp(-iqA_\alpha), \exp(-iqA_\beta))$  is therefore reduced to  $G = \text{diag}(\exp(-iqA), \exp(-iqA))$ . We are looking for an appropriate gauge field such that the covariant derivative becomes  $\mathcal{D}'_A \rightarrow \mathcal{D} + \mathcal{A}$  with the gauge transformation rule  $\mathcal{A}' = G\mathcal{A}G^\dagger - iG[\mathcal{D}_{dirac}, G^\dagger]$ . A convenient choice is [46–48]

$$\mathcal{A} = \begin{pmatrix} iq\gamma^\mu A_\mu^\alpha & 0 \\ 0 & iq\gamma^\mu A_\mu^\beta \end{pmatrix}. \quad (9)$$

$A_\mu^\alpha$  (respectively  $A_\mu^\beta$ ) is the magnetic vector potential  $A_\mu$  on the graphene layer  $\alpha$  (respectively  $\beta$ ). According to the appropriate covariant derivative, the introduction of the gauge field in equation (7) leads to [46–48]

$$\begin{pmatrix} i\gamma^\mu(\partial_\mu + iqA_\mu^\alpha) - m & ig\gamma^5 \\ ig\gamma^5 & i\gamma^\mu(\partial_\mu + iqA_\mu^\beta) - m \end{pmatrix} \begin{pmatrix} \psi_\alpha \\ \psi_\beta \end{pmatrix} = 0. \quad (10)$$

Of course, for graphene sheets, we have  $x_3 = 0$ , which corresponds to two bidimensional sheets instead of three-dimensional space sheets. In addition, we will assume that  $A_\mu$  is parallel to graphene layers ( $A_3 = 0$ ).

### 4 K-K' couplings in twisted graphene layers

In braneworld models, we simply have to consider the interaction between one fermion and domain walls described by a scalar field [46]. By contrast, a bilayer graphene is formally a many-body problem. Therefore we should normally consider the whole dynamics of carbon atoms and their electrons. This would be a very complicated task of course. As a consequence, we use the common tight-binding approach [3–17] to show the shared formalism between graphene bilayer and two-sheeted spacetime.

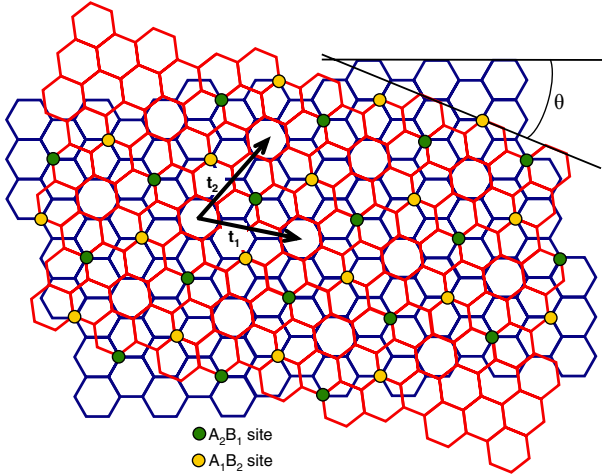


**Fig. 2.** Sketch of the two twisted graphene layers under consideration. Both sheets are rotated with respect to each other with an angle  $\theta \approx 21.787^\circ$ .  $\mathbf{t}_1$  and  $\mathbf{t}_2$  are the vectors of the Moiré unit cell.

Moreover, the existence of coupling terms proportional to  $g$  is straightforward for turbostratic graphene layers as explained hereafter. When two graphene layers are twisted with respect to each other, a typical Moiré pattern can be observed [3–9] (Fig. 2). This occurs when both layers are commensurate, i.e. when two specific kind of atoms of each layer can be superimposed periodically [3–9]. The Moiré pattern can be then described through a periodic unit cell defined by vectors  $\mathbf{t}_1$  and  $\mathbf{t}_2$  (see Fig. 2) and can only exist for a specific rotation angle  $\theta = \theta_{p,q}$  (with  $p, q \in \mathbb{N}$ ) between both layers.

Let us define  $\mathbf{a}_1 = a_0(1/2, \sqrt{3}/2)$  and  $\mathbf{a}_2 = a_0(-1/2, \sqrt{3}/2)$ , the vectors of the real space which define the unit cell of the first graphene layer (see Fig. 1a).  $a_0$  is the lattice parameter. Two kinds of commensurate structures can be considered [3–5]. The first one is such that the vectors of the Moiré unit cell are  $\mathbf{t}_1 = p\mathbf{a}_1 + (p+q)\mathbf{a}_2$  and  $\mathbf{t}_2 = -(p+q)\mathbf{a}_1 + (2p+q)\mathbf{a}_2$  such that  $\gcd(q, 3) = 1$ . The second case is such that  $\mathbf{t}_1 = (p+q/3)\mathbf{a}_1 + (q/3)\mathbf{a}_2$  and  $\mathbf{t}_2 = -(q/3)\mathbf{a}_1 + (p+2q/3)\mathbf{a}_2$  with  $\gcd(q, 3) = 3$ . In both cases, the rotation angle  $\theta_{p,q}$  between both sheets is given by [3–5]:

$$\cos \theta_{p,q} = \frac{3p^2 + 3pq + q^2/2}{3p^2 + 3pq + q^2}. \quad (11)$$

In the first layer, the first  $K$  Dirac cone is located at  $\mathbf{K} = (4\pi/(3a_0))(1, 0)$  while the  $K'$  Dirac cone is at  $\mathbf{K}' = -\mathbf{K}$ . By contrast, in the second layer, due to the rotation the  $K$  Dirac cone is located at  $\mathbf{K}^\theta = (4\pi/(3a_0))(\cos \theta, \sin \theta)$  whenever the  $K'$  Dirac cone is at  $\mathbf{K}'^\theta = -\mathbf{K}^\theta$  [3–5]. Let  $\mathbf{G}_1$  and  $\mathbf{G}_2$  be the vectors of the unit cell of the reciprocal lattice of the Moiré pattern. Obviously, the Moiré pattern can be responsible for coupling between valleys of each layer [3–9]. Indeed, we get

$$\mathbf{G} = \mathbf{K} - \mathbf{K}^\theta = -(\mathbf{K}' - \mathbf{K}'^\theta) \quad (12)$$

for  $K$ - $K'$  couplings, and

$$\mathbf{G}_c = \mathbf{K} - \mathbf{K}'^\theta = -(\mathbf{K}' - \mathbf{K}^\theta) \quad (13)$$

for  $K$ - $K'$  couplings. When  $\gcd(q, 3) = 1$ , then  $\mathbf{G} = -(q/3)(2\mathbf{G}_1 + \mathbf{G}_2)$  and  $\mathbf{G}_c = -(2p+q)\mathbf{G}_2$ . While, when  $\gcd(q, 3) = 3$ , then  $\mathbf{G} = -(q/3)(\mathbf{G}_1 + \mathbf{G}_2)$  and  $\mathbf{G}_c = (1/3)(2p+q)(\mathbf{G}_1 - \mathbf{G}_2)$ . The greater  $\mathbf{G}$  and  $\mathbf{G}_c$  are, the weaker the couplings are. As a consequence, one should consider the lowest values of  $p$  and  $q$ . A similar consideration leads us to expect that  $K$ - $K'$  interlayer couplings are usually stronger than the  $K$ - $K'$  ones. Then, for the purposes of our study, it should be relevant to consider a structure which can suppress the  $K$ - $K'$  couplings while enhancing the  $K$ - $K'$  interlayer couplings. We may consider for instance the case such that  $\gcd(q, 3) = 1$  with  $q = 1$ . Indeed, in that case  $\mathbf{G} = -(1/3)(2\mathbf{G}_1 + \mathbf{G}_2)$  is not a vector of the reciprocal lattice. By contrast  $\mathbf{G}_c = -(2p+1)\mathbf{G}_2$  is always a vector of the reciprocal lattice and is such that  $G_c \approx 2K$  whatever  $p$ . The first relevant value to be considered is then  $p = 1$ . In this case,  $\theta_{1,1} \approx 21.787^\circ$  and we obtain the specific structure shown in Figure 2. Of course, other angles  $\theta_{p,q}$  lower than  $\theta_{1,1}$  could be considered. But without loss of generality, we choose the case  $\theta = \theta_{1,1}$  to illustrate our topic.

Let us now justify the use of the noncommutative two-sheeted Dirac equation thanks to a solid-state approach. The whole detailed calculations are given in Appendix A and we focus below on the heuristic arguments. In a tight-binding approach it is possible to define the operator  $a_{\alpha(\beta),j}^\dagger$  (respectively  $a_{\alpha(\beta),j}$ ), which creates an electron (respectively a hole) on the site  $j$  of the sublattice “A” on the  $\alpha$  graphene layer (or on the  $\beta$  graphene layer). The same convention is used for the sublattice “B”. If one considers the interlayer coupling, one gets for the twisted system [3–10]:

$$H_c = - \sum_j t_{AB,j} a_{\alpha,j}^\dagger b_{\beta,j} - \sum_j t_{BA,j} b_{\alpha,j}^\dagger a_{\beta,j} + H.c. \quad (14)$$

where the energies  $t_{uv,j}$  (with  $u = A, B$  and  $v = A, B$ ) are related to the interlayer hopping between the nearest sites of each layer. This dependence of  $t_{uv,j}$  vs. the location  $j$  is very specific for two turbostratic graphene layers. In the structure considered here, we can see that no  $AA$  site exists by contrast to the  $AB$  sites (Fig. 2). We then assume that  $t_{AA,j} \approx t_{BB,j} \approx 0$ . In addition,  $t_{AB}(\mathbf{R}_j) = t_{AB,j} = -t'$  when  $\mathbf{R}_j = (2/3)(\mathbf{t}_1 + \mathbf{t}_2) + (n\mathbf{t}_1 + m\mathbf{t}_2)$  (with  $\mathbf{t}_1 = \mathbf{a}_1 + 2\mathbf{a}_2$  and  $\mathbf{t}_2 = -2\mathbf{a}_1 + 3\mathbf{a}_2$ ) and  $t_{BA}(\mathbf{R}_j) = t_{BA,j} = -t'$  when  $\mathbf{R}_j = (1/3)(\mathbf{t}_1 + \mathbf{t}_2) + (n\mathbf{t}_1 + m\mathbf{t}_2)$ , with  $n, m \in \mathbb{N}$ .  $t_{AB,j}$  and  $t_{BA,j}$  are equal to zero elsewhere. We use the following Fourier transform of the operators:

$$a_{\alpha(\beta)}(\mathbf{r}_j) = a_{\alpha(\beta),j} = \sum_k \frac{1}{\sqrt{N}} a_{\alpha(\beta),\mathbf{q}_k} e^{i\mathbf{r}_j^{(\prime)} \cdot \mathbf{q}_k^{(\prime)}} \quad (15)$$

with a similar convention for  $b_{\alpha(\beta),j}$  and where  $\mathbf{r}_i$  (respectively  $\mathbf{r}_i^{(\prime)}$ ) is the position vector of the site  $i$  in the first graphene layer ( $\alpha$ ) (respectively in the second graphene layer ( $\beta$ )). Then,  $\mathbf{q}_k$  (respectively  $\mathbf{q}_k^{(\prime)}$ ) is a momentum in

layer ( $\alpha$ ) (respectively ( $\beta$ )).  $N$  is the number of sites. Let us consider a single particle state with momentum  $\mathbf{k}$  such that we can consider the restricted Fourier representation of the Hamiltonian:  $H_c = H_{c,\mathbf{K}+\mathbf{k}} + H_{c,\mathbf{K}'+\mathbf{k}} + H_{c,\mathbf{K}''+\mathbf{k}} + H_{c,\mathbf{K}'''+\mathbf{k}}$  such that  $H_c = \Psi^\dagger \mathcal{H}_c \Psi$  with (see Appendix A):

$$\mathcal{H}_c = -i\hbar v_F \Gamma^0 \Gamma^5 D_5 + \hbar v_F \Gamma^3 D_6 \quad (16)$$

and

$$\begin{aligned} \Psi^t &= (a_{\alpha,K} \ b_{\alpha,K} \ a_{\alpha,K'} \ b_{\alpha,K'} \ a_{\beta,K} \ b_{\beta,K} \ a_{\beta,K'} \ b_{\beta,K'}) \\ &\sim (\psi_\alpha^t \ \psi_\beta^t) \end{aligned} \quad (17)$$

and where we have defined:

$$D_6 = \begin{pmatrix} 0 & \tilde{g} \\ -\tilde{g} & 0 \end{pmatrix} \quad (18)$$

by analogy with notations (5). The discussion about the precise meaning and the physical consequences of the  $D_6$  term is out of the present topic but deserves further works. In addition, the effective coupling constants are then given by  $g = (t'/v_F \hbar) \cos(\theta/2)$  and  $\tilde{g} = (t'/v_F \hbar) \sin(\theta/2)$ . Noticing that  $\tilde{g}/g = \tan(\theta/2)$ , since  $\theta \approx 21.787^\circ$  in our present case, we note that  $\tilde{g}/g \approx 0.2$ , i.e. the effective coupling constant  $\tilde{g}$  is five times lower than  $g$ . As a consequence, in the following we focus on the processes carried by the coupling constant  $g$ , and the remaining coupling Hamiltonian is:

$$\mathcal{H}_c = -iv_F \hbar \Gamma^0 \Gamma^5 D_5. \quad (19)$$

Using the above notations, the Lagrangian term related to  $\mathcal{H}_c$  in Dirac notation then becomes  $\mathcal{L}_c = \bar{\Psi} i \Gamma^5 D_5 \Psi$ , i.e. equation (8) related to equation (7).

Now, the coupling constant  $g$  can be then defined as  $g \approx t'/\hbar v_F$  and the phenomenological distance is  $\delta = \hbar v_F/t'$ . Basically,  $g$  and  $\delta$  must depend on the real distance  $d$  between each graphene sheet. Indeed, the hopping energy  $t'$  varies as [9]:  $t' \sim t_0 \exp(5.43(1 - d/a_m))$ , with  $t_0 \approx 0.3$  eV [2,9,10], and here  $d$  is the distance between two layers, while  $a_m$  is the nearest interlayer distance,  $a_m = 3.35$  Å. For closest layers ( $d = a_m$ ), we get  $\delta$  of about 22 Å (i.e.  $g \approx 4.5 \times 10^8$  m<sup>-1</sup>). As an indication, note that for  $d = 2a_m$  (respectively  $d = 5a_m$ ), one gets  $g \approx 2 \times 10^6$  m<sup>-1</sup> (respectively  $g \approx 1.7 \times 10^{-1}$  m<sup>-1</sup>).

## 5 Phenomenology of the model

Following previous works [46–48], we focus on the nonrelativistic limit of our Dirac like equation. Defining  $\nabla = (\partial_1, \partial_2)$ ,  $\mathbf{A} = (A_1, A_2)$ ,  $\boldsymbol{\sigma} = (\sigma_1, \sigma_2)$  and  $B_3 = \partial_1 A_2 - \partial_2 A_1$  and using:

$$F_{A(B)} = \begin{pmatrix} \chi_{A(B)} \\ \theta_{A(B)} \end{pmatrix},$$

and following the well-known standard procedure, a two-layer Pauli equation can be derived from equation (10) [46–49]:

$$i\hbar \frac{\partial}{\partial t} \begin{pmatrix} F_{A,\alpha} \\ F_{A,\beta} \end{pmatrix} = \{\mathbf{H}_0 + \mathbf{H}_{cm}\} \begin{pmatrix} F_{A,\alpha} \\ F_{A,\beta} \end{pmatrix}, \quad (20)$$

where  $F_{A,\alpha}$  and  $F_{A,\beta}$  correspond to the wave functions in the graphene layers  $\alpha$  and  $\beta$ , respectively. The Hamiltonian  $\mathbf{H}_0$  is a block-diagonal matrix such that  $\mathbf{H}_0 = \text{diag}(\mathbf{H}_\alpha, \mathbf{H}_\beta)$ , where each block is simply the effective Pauli Hamiltonian expressed in each graphene layer [46–49]:

$$\mathbf{H}_{\alpha(\beta)} = -\frac{\hbar^2}{2m} \left( \nabla - i\frac{q}{\hbar} \mathbf{A}_{\alpha(\beta)} \right)^2 + \mu_3 B_{3,\alpha(\beta)} + V_{\alpha(\beta)} \quad (21)$$

such that  $\mathbf{A}_\alpha$  and  $\mathbf{A}_\beta$  correspond to the magnetic vector potentials on the layers  $\alpha$  and  $\beta$ , respectively. The same convention is applied to the magnetic fields  $\mathbf{B}_{\alpha(\beta)}$  and to the potentials  $V_{\alpha(\beta)}$ . In the following, since we consider neutral excitons, we can set  $V_{\alpha(\beta)} = 0$ . In addition, we will show hereafter that  $B_{3,\alpha(\beta)} = 0$  in the device under consideration (see Sect. 6). We set  $\boldsymbol{\mu} = \gamma(\hbar/2)\boldsymbol{\sigma}$ , where  $\gamma$  is the iso-gyromagnetic ratio and  $\boldsymbol{\mu}$  the iso-magnetic moment related to the isospin of the particle [35]. With this choice, the present approach can be extended to any particle endowed with a magnetic moment whatever its isospin value.

In addition to these usual terms, the two-layer graphene Hamiltonian comprises also a new specific term [46–49]:

$$\mathbf{H}_{cm} = \begin{pmatrix} 0 & -ig\boldsymbol{\mu} \cdot \{\mathbf{A}_\alpha - \mathbf{A}_\beta\} \\ ig\boldsymbol{\mu} \cdot \{\mathbf{A}_\alpha - \mathbf{A}_\beta\} & 0 \end{pmatrix}. \quad (22)$$

$\mathbf{H}_{cm}$  is obviously not conventional and describes the coupling of the layers through electromagnetic fields. It vanishes for null magnetic vector potentials. Intuitively, the coupling generated by this term will imply Rabi oscillations of electrons or holes between both graphene sheets due to electronic delocalization.

## 6 Exciton swapping between two graphene layers and experimental device

Guided by the previous equations, we now suggest an experimental approach for testing exciton swapping between two graphene layers. An incident electromagnetic wave with an appropriate energy can excite an electron-hole bound pair (i.e. an exciton) [29–34] on a first graphene layer ( $G_\alpha$ ). In the best of our knowledge, studies related to the magnetic moment of exciton in graphene are still lacking. Nevertheless, exciton should exhibit resonance states endowed with non-zero magnetic moment  $\boldsymbol{\mu}$  [57,58] due to the combination of the electron/hole magnetic moments [35], possibly supplemented by an orbital magnetic moment. One can then expect to induce a coupling through  $\mathbf{H}_{cm}$  between  $G_\alpha$  and a second graphene layer  $G_\beta$  leading to a swapping of the exciton from  $G_\alpha$  towards  $G_\beta$ . Afterwards, the exciton decay on the second layer could be recorded.

The required magnetic vector potentials can be produced with the following device. Let us consider two coaxial annular magnets coated with an insulating material (see Fig. 3a). Both magnets have the same rectangular

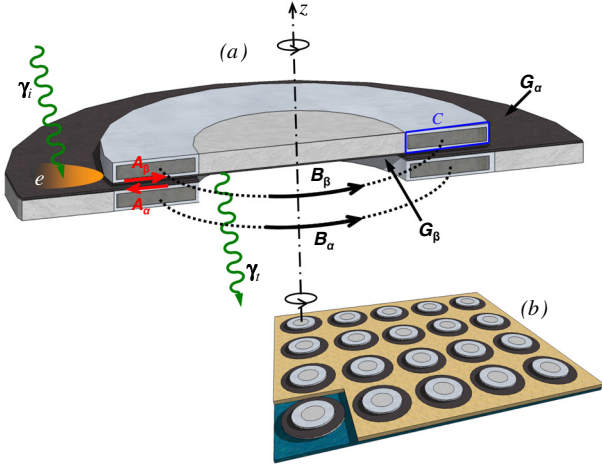


**Fig. 3.** Sketch of a feasible experimental setup. (a) Basic setup. Two coaxial annular magnets, with different inner and outer diameters, coated by an insulating material. The upper ring is filled up with an opaque material. Two magnetic fields ( $B_\alpha$  and  $B_\beta$ ) turn around the symmetry axis of the magnets. Two graphene layers ( $G_\alpha$  and  $G_\beta$ ) are considered, each one deposited on a face of a magnet. The geometry of the device allows for the existence of two opposite magnetic vector potentials  $A_\alpha$  and  $A_\beta$  (red arrows), each one in the vicinity of a graphene layer. An incident photon  $\gamma_i$  pumps an exciton  $e$  on  $G_\alpha$ . A photon  $\gamma_t$  resulting from the exciton decay on  $G_\beta$  can be recorded. (b) Full setup. Rectangular array of annular devices deposited on a transparent substrate (blue layer). The area between the toroidal magnets is filled with an opaque material (yellowish layer). Such a setup allows to enhance the recorded signal by increasing the graphene area.

section. Both magnetic fields ( $\mathbf{B}_\alpha$  and  $\mathbf{B}_\beta$ ) inside the magnets turn around the symmetry axis of the magnets.  $B_\alpha = B_\beta = 0$  outside the magnets due to the toroidal topology [59,60]. Only a magnetic vector potential  $\mathbf{A}$  exists outside the magnet [59,60] (i.e.  $\nabla \times \mathbf{A} = 0$ ). Boundary conditions result from  $\oint_C \mathbf{A} \cdot d\mathbf{l} = \Phi$ , where  $C$  is a contour on a magnet (see Fig. 3) and  $\Phi$  the magnetic flux inside a magnet. The geometry of the device leads to two opposite magnetic vector potentials ( $\mathbf{A}_\alpha$  and  $\mathbf{A}_\beta$ ), each one in the vicinity of a graphene layer ( $G_\alpha$  and  $G_\beta$ ) deposited on a face of a magnet (see Fig. 3a). A straightforward calculation shows that  $|\mathbf{A}_\alpha - \mathbf{A}_\beta| \sim 2A_0d/(L+l)$ , with  $d$  the distance between the two layers,  $L$  and  $l$  are the length and width of rectangular section of the magnets. If one considers a superconducting magnet, then  $A_0 \sim nh/(4e(L+l))$ , where  $n$  is an integer ( $h$  is the Planck constant and  $e$  the electric charge), due to the magnetic flux quantization [61]. For instance, if  $L = 1 \mu\text{m}$  and  $l = 10 \text{ nm}$  [59,60] and with  $d = 2a_m$ , one gets  $|\mathbf{A}_\alpha - \mathbf{A}_\beta| \approx 1.4 \times 10^{-12} \text{ T m}$  for  $n = 1$ .

The insulating material is the substrate on which the graphene layers are deposited. This allows a gated graphene leading to electrons and holes sharing the same effective mass [25,26]. The efficient graphene area can be increased by using a large array of micro-annular devices (see Fig. 3b).

The excitonic swapping can be described as follows. One looks for an exciton wave function in the form:

$$|\Phi(t)\rangle = \begin{pmatrix} F_{A,\alpha}(t) \\ F_{A,\beta}(t) \end{pmatrix} \quad (23)$$

$$= a_\alpha(t) \begin{pmatrix} \Psi_s \\ 0 \end{pmatrix} + a_\beta(t) \begin{pmatrix} 0 \\ \Psi_s \end{pmatrix},$$

where it is assumed that  $\mu\Psi_s = \pm\mu\Psi_s$ , i.e.  $\Psi_s$  is an eigenstate of  $\mu$  with an eigenvalue  $\mu$  different from zero. For an exciton, the lowest expected value can be estimated by  $\mu \sim e\hbar/m$  [57,58], i.e.  $\mu \approx 3.5 \times 10^{-22} \text{ J T}^{-1}$  for an effective electron/hole mass about 0.3 eV [25–27]. Note that such a value of the mass gap corresponds to a common order of magnitude for graphene on a substrate [25–28]. As a consequence, by choosing a value of 0.3 eV [25,26], we do not lose any generality. Putting equation (23) into the Pauli equation (20) leads to the following system of coupled differential equations:

$$\frac{d}{dt}a_\alpha = -\kappa a_\beta - (1/2)\Gamma_0 a_\alpha + \delta(t - t_i) \quad (24)$$

and

$$\frac{d}{dt}a_\beta = \kappa a_\alpha - (1/2)\Gamma_0 a_\beta \quad (25)$$

with  $\kappa = \mu g |\mathbf{A}_\alpha - \mathbf{A}_\beta| / \hbar$ . With the above mentioned values, one can roughly estimate  $\kappa \approx 2.1 \times 10^9 \text{ rad s}^{-1}$ .  $\Gamma_0$  is the exciton decay rate conveniently introduced in the equations in agreement with the lifetime  $\tau$  of the exciton ( $\Gamma_0 = \tau^{-1}$ ). We assume that  $\tau$  is comprised between 10 fs and 200 ps [33,62,63] ( $5 \times 10^9 \text{ s}^{-1} \leq \Gamma_0 \leq 10^{14} \text{ s}^{-1}$ ).  $\delta(t - t_i)$  is a Dirac delta source such that the exciton is created at  $t = t_i$  in the layer  $\alpha$ . Then,  $a_\alpha(t = t_i) = 1$  and  $a_\beta(t = t_i) = 0$ . The number of excitons is then given by  $\mathcal{N}_\alpha = \sum_i a_\alpha^* a_\alpha$  (respectively  $\mathcal{N}_\beta = \sum_i a_\beta^* a_\beta$ ) in layer  $\alpha$  (respectively in layer  $\beta$ ). In the continuous limit such that  $\mathcal{M}$  excitons are produced per second, from equations (24) and (25), one easily obtains three Bloch-like equations:

$$\frac{d}{dt}\mathcal{N}_\alpha = -\kappa\mathcal{U} - \Gamma_0\mathcal{N}_\alpha + \mathcal{M} \quad (26)$$

and

$$\frac{d}{dt}\mathcal{N}_\beta = \kappa\mathcal{U} - \Gamma_0\mathcal{N}_\beta \quad (27)$$

and

$$\frac{d}{dt}\mathcal{U} = 2\kappa\mathcal{N}_\alpha - 2\kappa\mathcal{N}_\beta - \Gamma_0\mathcal{U} \quad (28)$$

with  $\mathcal{U} = \sum_i (a_\alpha^* a_\beta + a_\alpha a_\beta^*)$ . Since layer  $\alpha$  is continuously supplied with new excitons thanks to an incident photon flux  $\mathcal{I}_0$ , the exciton source is such that  $\mathcal{M} = \rho_{\text{eff}}\mathcal{I}_0$ .  $\rho_{\text{eff}}$  is the photon-to-exciton conversion efficiency. Equations (26) to (28) must present short-time transient solutions due to  $-\Gamma_0\mathcal{N}_{\alpha(\beta)}$  and  $-\Gamma_0\mathcal{U}$  terms. As a consequence, we look for stationary solutions such that  $d\mathcal{N}_\alpha/dt = d\mathcal{N}_\beta/dt = d\mathcal{U}/dt = 0$ . Equations (26) to (28) can be then trivially solved. The number of excitons in each graphene layers are:

$$\mathcal{N}_\alpha = \frac{2\kappa^2 + \Gamma_0^2}{\Gamma_0(4\kappa^2 + \Gamma_0^2)}\mathcal{M}, \text{ and } \mathcal{N}_\beta = \frac{2\kappa^2}{\Gamma_0(4\kappa^2 + \Gamma_0^2)}\mathcal{M} \quad (29)$$

and the number of newly created excitons balances the number of decaying excitons, i.e.  $\mathcal{M} = \Gamma_0 (\mathcal{N}_\alpha + \mathcal{N}_\beta)$ . Note that in the present approach, we do not consider any saturation effect regarding to the number of excitons per unit area. Then for a fixed area,  $\mathcal{N}_\alpha + \mathcal{N}_\beta$  should be limited and  $\mathcal{M}/\Gamma_0$  likewise. As a consequence, for a given value of  $\mathcal{M}$ , the present approach is not valid when  $\Gamma_0 \rightarrow 0$ .

The photon flux  $\mathcal{I}_t$  emitted from the second graphene layer  $\beta$  is  $\mathcal{I}_t = n\Gamma_0\mathcal{N}_\beta$  where  $n$  is the number of photons that results from the exciton decay. The effective optical transmission coefficient  $\mathcal{T}$  of the device is  $\mathcal{T} = \mathcal{I}_t/\mathcal{I}_0$ , and one gets:

$$\mathcal{T} = n\rho_{\text{eff}} \frac{2\kappa^2}{4\kappa^2 + \Gamma_0^2}. \quad (30)$$

The excitons transferred from layer  $\alpha$  to layer  $\beta$  are then detected through recorded photons due to excitonic decay (see Fig. 3a). Let us consider the simplest process such that  $n\rho_{\text{eff}} = 1$ , i.e. every exciton decays into a single photon, and each photon creates a single exciton [64,65]. With the above values, the best expected transmission  $\mathcal{T}$  could reach 21%, which is of course a fair value in an experimental context.

## 7 Conclusions

Using a theoretical approach previously considered to describe a Universe made of two braneworlds [46–49], we have proposed a new theoretical description of the phenomenology of two twisted graphene sheets. The model considers that some graphene bilayers can be described by a two-sheeted  $(2+1)$ -spacetime in the formalism of the noncommutative geometry. The model has been justified by means of a tight-binding approach, and the noncommutative geometry emerges from  $K$ - $K'$  couplings between graphene layers. This suggests a new way to describe multilayer graphene, which deserves further studies. We have shown that the transfer of excitons between the two graphene sheets is allowed for some specific electromagnetic conditions. While the excitons are produced by incident light on the first graphene layer, photons could be recorded in front of the second graphene layer where the swapped exciton decays. The suggested experimental device uses magnets whose magnetic fields can be controlled with a transient external magnetic field, allowing then to turn on or off the device. We can then expect to get a new kind of electro-optic light modulator with hysteresis. The described effect is a solid-state realization of a two-brane Universe, for which it has been shown that matter swapping between two braneworlds could occur [46–49]. As a consequence, any experimental evidence of this effect in graphene bilayers would also be relevant in the outlook of braneworld studies.

## Appendix A: Effective two-sheeted Hamiltonian

Let us justify equations (7) and (19), and so the noncommutative formalism used to describe the two graphene

sheets. We consider a tight-binding approach. One defines the operator  $a_{\alpha(\beta),j}^\dagger$  (respectively  $a_{\alpha(\beta),j}$ ) which creates an electron (a hole) on the site  $j$  of the sublattice “A” on the  $\alpha$  graphene layer (or the  $\beta$  graphene layer). The same convention is used for the sublattice “B”. The Hamiltonian for the bilayer can be then written as  $H = H_\alpha + H_\beta + H_c$  with:

$$H_{\alpha(\beta)} = \sum_j \left( \varepsilon_A a_{\alpha(\beta),j}^\dagger a_{\alpha(\beta),j} + \varepsilon_B b_{\alpha(\beta),j}^\dagger b_{\alpha(\beta),j} \right) - t \sum_{\langle i,j \rangle} \left( a_{\alpha(\beta),i}^\dagger b_{\alpha(\beta),j} + b_{\alpha(\beta),j}^\dagger a_{\alpha(\beta),i} \right). \quad (A.1)$$

$H_{\alpha(\beta)}$  are simply the Hamiltonian of each graphene sheet ( $\alpha$ ) and ( $\beta$ ).  $\varepsilon_A$  (respectively  $\varepsilon_B$ ) is the energy level of the electron in a site of the sublattice “A” (respectively “B”).  $t$  is the energy related to nearest-neighbour hopping.  $\langle i,j \rangle$  corresponds to the sum over all sites  $j$  and their nearest neighbours  $i$ . If one considers the interlayer coupling, one gets:

$$H_c = - \sum_j t_{AA,j} \left( a_{\alpha,j}^\dagger a_{\beta,j} + a_{\beta,j}^\dagger a_{\alpha,j} \right) - \sum_j t_{BB,j} \left( b_{\alpha,j}^\dagger b_{\beta,j} + b_{\beta,j}^\dagger b_{\alpha,j} \right) - \sum_j t_{AB,j} \left( a_{\alpha,j}^\dagger b_{\beta,j} + b_{\beta,j}^\dagger a_{\alpha,j} \right) - \sum_j t_{BA,j} \left( b_{\alpha,j}^\dagger a_{\beta,j} + a_{\beta,j}^\dagger b_{\alpha,j} \right) \quad (A.2)$$

where the energies  $t_{uv,j}$  (with  $u = A, B$  and  $v = A, B$ ) denote the interlayer hopping between each nearest site of each layer. This dependence of  $t_{uv,j}$  against the location  $j$  is specific for a coupling between two turbostratic graphene layers for instance. In the structure considered here, we can see that no  $AA$  ( $BB$ ) site exists by contrast to the  $AB$  ( $BA$ ) sites (see Fig. 2). We then assume that  $t_{AA,j} \approx t_{BB,j} \approx 0$ . In addition,  $t_{AB}(\mathbf{R}_j) = t_{AB,j} = -t'$  when  $\mathbf{R}_j = (2/3)(\mathbf{t}_1 + \mathbf{t}_2) + (n\mathbf{t}_1 + m\mathbf{t}_2)$  (with  $\mathbf{t}_1 = \mathbf{a}_1 + 2\mathbf{a}_2$  and  $\mathbf{t}_2 = -2\mathbf{a}_1 + 3\mathbf{a}_2$ ) and  $t_{BA}(\mathbf{R}_j) = t_{BA,j} = -t'$  when  $\bar{\mathbf{R}}_j = (1/3)(\mathbf{t}_1 + \mathbf{t}_2) + (n\mathbf{t}_1 + m\mathbf{t}_2)$ , with  $n, m \in \mathbb{N}$ .  $t_{AB,j}$  and  $t_{BA,j}$  are equal to zero elsewhere. As a consequence  $H_c$  becomes:

$$H_c = t' \sum_{[j]} \left( a_{\alpha,j}^\dagger b_{\beta,j} + b_{\beta,j}^\dagger a_{\alpha,j} \right) + t' \sum_{[j]} \left( b_{\alpha,j}^\dagger a_{\beta,j} + a_{\beta,j}^\dagger b_{\alpha,j} \right), \quad (A.3)$$

where  $[j]$  corresponds to the sum over all sites  $\mathbf{R}_j$  or  $\bar{\mathbf{R}}_j$ . We then use the following Fourier transform of the operators:

$$a(b)_{\alpha,j} = \sum_k \frac{1}{\sqrt{N}} a(b)_{\alpha,\mathbf{q}_k} e^{i\mathbf{r}_j \cdot \mathbf{q}_k} \quad (A.4)$$

$$a(b)_{\beta,j} = \sum_k \frac{1}{\sqrt{N}} a(b)_{\beta,\mathbf{q}'_k} e^{i\mathbf{r}'_j \cdot \mathbf{q}'_k} \quad (A.5)$$

where  $\mathbf{r}_i$  (respectively  $\mathbf{r}'_i$ ) is the position vector of the site  $i$  in the first graphene layer ( $\alpha$ ) (respectively in the second graphene layer ( $\beta$ )). Then,  $\mathbf{q}_k$  (respectively  $\mathbf{q}'_k$ ) is a momentum in layer ( $\alpha$ ) (respectively ( $\beta$ )).  $N$  is the number of sites. We can then write  $H = \sum_k H_k$ , and we get:

$$\begin{aligned}
H = & \left( \varepsilon_A \sum_k a_{\alpha, \mathbf{q}_k}^\dagger a_{\alpha, \mathbf{q}_k} + \varepsilon_B \sum_k b_{\alpha, \mathbf{q}_k}^\dagger b_{\alpha, \mathbf{q}_k} \right. \\
& - t \sum_k a_{\alpha, \mathbf{q}_k}^\dagger b_{\alpha, \mathbf{q}_k} [e^{i\mathbf{u}_1 \cdot \mathbf{q}_k} + e^{i\mathbf{u}_2 \cdot \mathbf{q}_k} + e^{i\mathbf{u}_3 \cdot \mathbf{q}_k}] \\
& \left. - t \sum_k b_{\alpha, \mathbf{q}_k}^\dagger a_{\alpha, \mathbf{q}_k} [e^{-i\mathbf{u}_1 \cdot \mathbf{q}_k} + e^{-i\mathbf{u}_2 \cdot \mathbf{q}_k} + e^{-i\mathbf{u}_3 \cdot \mathbf{q}_k}] \right) \\
& + \left( \varepsilon_A \sum_k a_{\beta, \mathbf{q}'_k}^\dagger a_{\beta, \mathbf{q}'_k} + \varepsilon_B \sum_k b_{\beta, \mathbf{q}'_k}^\dagger b_{\beta, \mathbf{q}'_k} \right. \\
& - t \sum_k a_{\beta, \mathbf{q}'_k}^\dagger b_{\beta, \mathbf{q}'_k} [e^{i\mathbf{u}'_1 \cdot \mathbf{q}'_k} + e^{i\mathbf{u}'_2 \cdot \mathbf{q}'_k} + e^{i\mathbf{u}'_3 \cdot \mathbf{q}'_k}] \\
& \left. - t \sum_k b_{\beta, \mathbf{q}'_k}^\dagger a_{\beta, \mathbf{q}'_k} [e^{-i\mathbf{u}'_1 \cdot \mathbf{q}'_k} + e^{-i\mathbf{u}'_2 \cdot \mathbf{q}'_k} + e^{-i\mathbf{u}'_3 \cdot \mathbf{q}'_k}] \right) \\
& + t' \sum_k \sum_{k'} a_{\alpha, \mathbf{q}_k}^\dagger b_{\beta, \mathbf{q}'_{k'}} \frac{1}{N} \sum_{[j]} e^{i\mathbf{r}'_j \cdot \mathbf{q}'_{k'} - i\mathbf{r}_j \cdot \mathbf{q}_k} \\
& + t' \sum_k \sum_{k'} b_{\beta, \mathbf{q}'_{k'}}^\dagger a_{\alpha, \mathbf{q}_k} \frac{1}{N} \sum_{[j]} e^{-i\mathbf{r}'_j \cdot \mathbf{q}'_{k'} + i\mathbf{r}_j \cdot \mathbf{q}_k} \\
& + t' \sum_k \sum_{k'} b_{\alpha, \mathbf{q}_k}^\dagger a_{\beta, \mathbf{q}'_{k'}} \frac{1}{N} \sum_{[j]} e^{i\mathbf{r}'_j \cdot \mathbf{q}'_{k'} - i\mathbf{r}_j \cdot \mathbf{q}_k} \\
& + t' \sum_k \sum_{k'} a_{\beta, \mathbf{q}'_{k'}}^\dagger b_{\alpha, \mathbf{q}_k} \frac{1}{N} \sum_{[j]} e^{-i\mathbf{r}'_j \cdot \mathbf{q}'_{k'} + i\mathbf{r}_j \cdot \mathbf{q}_k} \quad (\text{A.6})
\end{aligned}$$

since

$$\sum_{\langle i, j \rangle} e^{j(\mathbf{r}_j \cdot \mathbf{q}_{k'} - \mathbf{r}_i \cdot \mathbf{q}_k)} = N \delta_{\mathbf{q}_{k'}, \mathbf{q}_k} \sum_{j=1,2,3} e^{i\mathbf{u}_j \cdot \mathbf{q}_{k'}}$$

with

$$\mathbf{u}_1 = \mathbf{a}_2 - \mathbf{a}_1, \quad \mathbf{u}_2 = \mathbf{a}_1 \quad \text{and} \quad \mathbf{u}_3 = -\mathbf{a}_2.$$

Indeed, for a site  $i$  located at  $\mathbf{r}_i$ , the three nearest neighbours are located at  $\mathbf{r}_j = \mathbf{r}_i + \mathbf{u}_1$ ,  $\mathbf{r}_i + \mathbf{u}_2$  and  $\mathbf{r}_i + \mathbf{u}_3$  respectively. In the second graphene layer, the nearest neighbours are defined through  $\mathbf{u}'_i = \mathbf{R}(\theta)\mathbf{u}_i$ , with

$$\mathbf{R}(\theta) = \begin{pmatrix} \cos \theta & -\sin \theta \\ \sin \theta & \cos \theta \end{pmatrix}.$$

Let us now consider the restricted Hamiltonian  $\tilde{H}$  which only contains the contributions of the Hamiltonian  $H$  for

$\mathbf{q}_k \approx \mathbf{K}$  or  $\mathbf{K}'$ , and  $\mathbf{q}'_k \approx \mathbf{K}^\theta$  or  $\mathbf{K}'^\theta$ . Since:

$$\begin{aligned}
\sum_{[j]} e^{i\mathbf{r}'_j \cdot \mathbf{q}'_{k'} - i\mathbf{r}_j \cdot \mathbf{q}_k} &= \sum_j e^{i\mathbf{R}_j \cdot (\mathbf{K}'^\theta - \mathbf{K})} \\
&= e^{i(2/3)(\mathbf{t}_1 + \mathbf{t}_2) \cdot (\mathbf{K}'^\theta - \mathbf{K})} \\
&\quad \times \sum_{n,m} e^{i(n\mathbf{t}_1 + m\mathbf{t}_2) \cdot (\mathbf{K}'^\theta - \mathbf{K})} \\
&= N \quad (\text{A.7})
\end{aligned}$$

and

$$\begin{aligned}
\sum_{[j]} e^{i\mathbf{r}'_j \cdot \mathbf{q}'_{k'} - i\mathbf{r}_j \cdot \mathbf{q}_k} &= \sum_j e^{i\bar{\mathbf{R}}_j \cdot (\mathbf{K}'^\theta - \mathbf{K})} \\
&= e^{i(1/3)(\mathbf{t}_1 + \mathbf{t}_2) \cdot (\mathbf{K}'^\theta - \mathbf{K})} \\
&\quad \times \sum_{n,m} e^{i(n\mathbf{t}_1 + m\mathbf{t}_2) \cdot (\mathbf{K}'^\theta - \mathbf{K})} \\
&= N \quad (\text{A.8})
\end{aligned}$$

we can write  $\tilde{H}$  such that  $\tilde{H} = \Psi^{(\theta)\dagger} \mathcal{H}^{(\theta)} \Psi^{(\theta)}$  with

$$\mathcal{H}^{(\theta)} = \begin{pmatrix} \varepsilon_A & -t\Lambda_{\mathbf{K}}^* & 0 & 0 & 0 & 0 & 0 & t' \\ -t\Lambda_{\mathbf{K}} & \varepsilon_B & 0 & 0 & 0 & 0 & t' & 0 \\ 0 & 0 & \varepsilon_A & -t\Lambda_{\mathbf{K}'}^* & 0 & t' & 0 & 0 \\ 0 & 0 & -t\Lambda_{\mathbf{K}'} & \varepsilon_B & t' & 0 & 0 & 0 \\ 0 & 0 & 0 & t' & \varepsilon_A & -t\Lambda_{\mathbf{K}^\theta}^* & 0 & 0 \\ 0 & 0 & t' & 0 & -t\Lambda_{\mathbf{K}^\theta} & \varepsilon_B & 0 & 0 \\ 0 & t' & 0 & 0 & 0 & 0 & \varepsilon_A & -t\Lambda_{\mathbf{K}'^\theta}^* \\ t' & 0 & 0 & 0 & 0 & 0 & -t\Lambda_{\mathbf{K}'^\theta} & \varepsilon_B \end{pmatrix} \quad (\text{A.9})$$

where the star denotes the complex conjugate and

$$\begin{aligned}
\Lambda_{\mathbf{K}} &= \sum_i e^{i\mathbf{u}_i \cdot (\mathbf{K} + \mathbf{k})}, \quad \Lambda_{\mathbf{K}'} = \sum_i e^{i\mathbf{u}_i \cdot (\mathbf{K}' + \mathbf{k})}, \\
\Lambda_{\mathbf{K}^\theta} &= \sum_i e^{i\mathbf{u}'_i \cdot (\mathbf{K}^\theta + \mathbf{k})}.
\end{aligned}$$

and

$$\Lambda_{\mathbf{K}'^\theta} = \sum_i e^{i\mathbf{u}'_i \cdot (\mathbf{K}'^\theta + \mathbf{k})}.$$

$\mathbf{k}$  is the momentum vector which denotes low-energy excitations near the Dirac points. We also define:

$$\tilde{\Psi}^{(\theta)} = \begin{pmatrix} a_{\alpha, \mathbf{K}} \\ b_{\alpha, \mathbf{K}} \\ a_{\alpha, \mathbf{K}'} \\ b_{\alpha, \mathbf{K}'} \\ a_{\beta, \mathbf{K}^\theta} \\ b_{\beta, \mathbf{K}^\theta} \\ a_{\beta, \mathbf{K}'^\theta} \\ b_{\beta, \mathbf{K}'^\theta} \end{pmatrix} = \begin{pmatrix} \chi_\alpha \\ \theta_\alpha^{(\theta)} \\ \chi_\beta \\ \theta_\beta^{(\theta)} \end{pmatrix}. \quad (\text{A.10})$$

$$\mathcal{H}^{(\theta)} = \begin{pmatrix} \hbar v_F (\sigma_1 k_x + \sigma_2 k_y) + m v_f^2 \sigma_3 & 0 & 0 & t' \sigma_1 \\ 0 & \hbar v_F (-\sigma_1 k_x + \sigma_2 k_y) + m v_f^2 \sigma_3 & t' \sigma_1 & 0 \\ 0 & t' \sigma_1 & \hbar v_F (\sigma_1^\theta k_x + \sigma_2^\theta k_y) + m v_f^2 \sigma_3 & 0 \\ t' \sigma_1 & 0 & 0 & \hbar v_F (-\sigma_1^{-\theta} k_x + \sigma_2^{-\theta} k_y) + m v_f^2 \sigma_3 \end{pmatrix} \quad (\text{A.11})$$

$$\mathcal{H} = \begin{pmatrix} \hbar v_F (\sigma_1 k_x + \sigma_2 k_y) + m v_f^2 \sigma_3 & 0 & 0 & t' \sigma_1 e^{-i(\theta/2)\sigma_3} \\ 0 & \hbar v_F (-\sigma_1 k_x + \sigma_2 k_y) + m v_f^2 \sigma_3 & t' \sigma_1 e^{i(\theta/2)\sigma_3} & 0 \\ 0 & t' e^{-i(\theta/2)\sigma_3} \sigma_1 & \hbar v_F (\sigma_1 k_x + \sigma_2 k_y) + m v_f^2 \sigma_3 & 0 \\ t' e^{i(\theta/2)\sigma_3} \sigma_1 & 0 & 0 & \hbar v_F (-\sigma_1 k_x + \sigma_2 k_y) + m v_f^2 \sigma_3 \end{pmatrix} \quad (\text{A.14})$$

$$\mathcal{H} = \begin{pmatrix} \hbar v_F (\sigma_1 k_x + \sigma_2 k_y) + m v_f^2 \sigma_3 & 0 & 0 & -t' \sigma_2 e^{-i(\theta/2)\sigma_3} \\ 0 & \hbar v_F (\sigma_1 k_x - \sigma_2 k_y) + m v_f^2 \sigma_3 & -t' \sigma_2 e^{i(\theta/2)\sigma_3} & 0 \\ 0 & -t' e^{-i(\theta/2)\sigma_3} \sigma_2 & \hbar v_F (\sigma_1 k_x + \sigma_2 k_y) + m v_f^2 \sigma_3 & 0 \\ -t' e^{i(\theta/2)\sigma_3} \sigma_2 & 0 & 0 & \hbar v_F (\sigma_1 k_x - \sigma_2 k_y) + m v_f^2 \sigma_3 \end{pmatrix} \quad (\text{A.15})$$

Since  $|\mathbf{k}|$  can be assumed small enough, one gets the following first-order perturbation series by respect with  $\mathbf{k}$ :

$$\begin{aligned} \Lambda_{\mathbf{K}} &= -a_0 \frac{\sqrt{3}}{2} \{ \mathbf{e}_x \cdot \mathbf{k} + i \mathbf{e}_y \cdot \mathbf{k} \}, \\ \Lambda_{\mathbf{K}'} &= -a_0 \frac{\sqrt{3}}{2} \{ -\mathbf{e}_x \cdot \mathbf{k} + i \mathbf{e}_y \cdot \mathbf{k} \}, \\ \Lambda_{\mathbf{K}^\theta} &= -a_0 \frac{\sqrt{3}}{2} \{ \mathbf{R}(\theta) \mathbf{e}_x \cdot \mathbf{k} + i \mathbf{R}(\theta) \mathbf{e}_y \cdot \mathbf{k} \}, \end{aligned}$$

and

$$\Lambda_{\mathbf{K}'^\theta} = -a_0 \frac{\sqrt{3}}{2} \{ -\mathbf{R}(\theta) \mathbf{e}_x \cdot \mathbf{k} + i \mathbf{R}(\theta) \mathbf{e}_y \cdot \mathbf{k} \}.$$

Then, we can write:

*see equation (A.11) above,*

where  $v_F = \sqrt{3}at/2\hbar$  is the Fermi velocity. We have set  $m v_f^2 = (\varepsilon_A - \varepsilon_B)/2$ . The energy origin is defined as  $(\varepsilon_A + \varepsilon_B)/2 = 0$ . We have defined  $\sigma_i^\theta = e^{i(\theta/2)\sigma_3} \sigma_i e^{-i(\theta/2)\sigma_3}$ . Since

$$\Psi^{(\theta)} = \begin{pmatrix} \chi_\alpha \\ \theta_\alpha \\ \chi_\beta^{(\theta)} \\ \theta_\beta^{(\theta)} \end{pmatrix} = \begin{pmatrix} \chi_\alpha \\ \theta_\alpha \\ e^{i(\theta/2)\sigma_z} \chi_\beta \\ e^{-i(\theta/2)\sigma_z} \theta_\beta \end{pmatrix} \quad (\text{A.12})$$

we now conveniently define  $\mathcal{H}$  thanks to:

$\tilde{H} = \Psi^{(\theta)\dagger} \mathcal{H}^{(\theta)} \Psi^{(\theta)} = \Psi^\dagger \mathcal{H} \Psi$ , with

$$\Psi = \begin{pmatrix} \chi_\alpha \\ \theta_\alpha \\ \chi_\beta \\ \theta_\beta \end{pmatrix} \quad (\text{A.13})$$

and we get:

*see equation (A.14) above.*

We now execute a convenient  $\pi/2$  rotation such that  $(x, y) \rightarrow (-y, x)$  and  $(k_x, k_y) \rightarrow (-k_y, k_x)$  leading to:

*see equation (A.15) above.*

Let us now rewrite the Schrödinger equation related to the Hamiltonian (A.15) in a Dirac-like form. We use the notations (3) such that:

$$\gamma^0 = \begin{pmatrix} \sigma_3 & 0 \\ 0 & \sigma_3 \end{pmatrix}, \quad (\text{A.16})$$

and we multiply first  $i\hbar\partial_t\Psi = \mathcal{H}\Psi$  on the left by  $\gamma^0 \otimes \mathbf{1}_{2 \times 2}$ . Using the relation:

$$e^{i(\theta/2)\sigma_3} = \cos(\theta/2) + i\sigma_3 \sin(\theta/2), \quad (\text{A.17})$$

and the properties of the Pauli matrices, we get:

*see equation (A.18) next page.*

$$i\hbar \begin{pmatrix} \gamma^0 & 0 \\ 0 & \gamma^0 \end{pmatrix} \partial_t \Psi =$$

$$\begin{pmatrix} \hbar v_F (i\sigma_2 k_x + (-i\sigma_1) k_y) + mv_f^2 & 0 & 0 & -t' (-i\sigma_1 \cos(\theta/2) + \sigma_3 \sigma_1 \sin(\theta/2)) \\ 0 & \hbar v_F (i\sigma_2 k_x + (i\sigma_1) k_y) + mv_f^2 & -t' (-i\sigma_1 \cos(\theta/2) - \sigma_3 \sigma_1 \sin(\theta/2)) & 0 \\ 0 & -t' (-i\sigma_1 \cos(\theta/2) - \sigma_3 \sigma_1 \sin(\theta/2)) & \hbar v_F (i\sigma_2 k_x + (-i\sigma_1) k_y) + mv_f^2 & 0 \\ -t' (-i\sigma_1 \cos(\theta/2) + \sigma_3 \sigma_1 \sin(\theta/2)) & 0 & 0 & \hbar v_F (i\sigma_2 k_x + (i\sigma_1) k_y) + mv_f^2 \end{pmatrix} \Psi \quad (\text{A.18})$$

$$i\hbar \begin{pmatrix} \gamma^0 & 0 \\ 0 & \gamma^0 \end{pmatrix} \partial_t \Psi = \begin{pmatrix} \hbar v_F (\gamma^1 k_x + \gamma^2 k_y) + mv_f^2 & -t' (i\gamma^5 \cos(\theta/2) - \gamma^0 \gamma^3 \sin(\theta/2)) \\ -t' (i\gamma^5 \cos(\theta/2) + \gamma^0 \gamma^3 \sin(\theta/2)) & \hbar v_F (\gamma^1 k_x + \gamma^2 k_y) + mv_f^2 \end{pmatrix} \Psi \quad (\text{A.21})$$

By using notations (3) and (4), such as:

$$\gamma^1 = \begin{pmatrix} i\sigma_2 & 0 \\ 0 & i\sigma_2 \end{pmatrix}, \quad \gamma^2 = \begin{pmatrix} -i\sigma_1 & 0 \\ 0 & i\sigma_1 \end{pmatrix} \quad (\text{A.19})$$

and

$$\gamma^3 = \begin{pmatrix} 0 & -\sigma_1 \\ \sigma_1 & 0 \end{pmatrix}, \quad -i\gamma^5 = \begin{pmatrix} 0 & i\sigma_1 \\ i\sigma_1 & 0 \end{pmatrix}, \quad (\text{A.20})$$

equation (A.18) can then be written as:

*see equation (A.21) above.*

Now, let us define  $m \rightarrow mv_F/\hbar$  and  $(x_0, x_1, x_2) = (v_F t, x, y)$ , as well as  $g = (t'/v_F \hbar) \cos(\theta/2)$  and  $\tilde{g} = (t'/v_F \hbar) \sin(\theta/2)$ . We also use the equivalence  $(k_1, k_2) \longleftrightarrow (-i\partial_1, -i\partial_2)$ , and then equation (A.21) can be written as:

$$\begin{pmatrix} i\gamma^\eta \partial_\eta - m & ig\gamma^5 - \gamma^0 \gamma^3 \tilde{g} \\ ig\gamma^5 + \gamma^0 \gamma^3 \tilde{g} & i\gamma^\eta \partial_\eta - m \end{pmatrix} \Psi = 0 \quad (\text{A.22})$$

with  $\eta = 0, 1, 2$ . (A.22) is the Dirac-like form of the Schrödinger equation related to the Hamiltonian (A.15). If we neglect the role of the coupling  $\tilde{g}$ , or if we consider the role of the coupling  $g$  only, obviously, equation (A.22) is the expected equation (7) for  $x_3 = 0$ .

Note that, if we consider the notations (6), i.e.:

$$\Gamma^\mu = \begin{pmatrix} \gamma^\mu & 0 \\ 0 & \gamma^\mu \end{pmatrix} \quad \text{and} \quad \Gamma^5 = \begin{pmatrix} \gamma^5 & 0 \\ 0 & -\gamma^5 \end{pmatrix} \quad (\text{A.23})$$

it can be easily shown from the previous equations that the coupling Hamiltonian  $\mathcal{H}_c$  between both graphene layers reduces to:

$$\mathcal{H}_c = -i\hbar v_F \Gamma^0 \Gamma^5 D_5 + \hbar v_F \Gamma^3 D_6 \quad (\text{A.24})$$

which is the equation (16), with:

$$D_5 = \begin{pmatrix} 0 & g \\ -g & 0 \end{pmatrix} \quad (\text{A.25})$$

from notations (5), and where we have defined:

$$D_6 = \begin{pmatrix} 0 & \tilde{g} \\ -\tilde{g} & 0 \end{pmatrix} \quad (\text{A.26})$$

by analogy with (A.25).

The authors are grateful to Philippe Lambin, Luc Henrard and Nicolas Reckinger for useful discussions and comments.

## References

1. K.S. Novoselov, A.K. Geim, S.V. Morozov, D. Jiang, M.I. Katsnelson, I.V. Grigorieva, S.V. Dubonos, A.A. Firsov, *Nature* **438**, 197 (2005)
2. A.H. Castro Neto, F. Guinea, N.M.R. Peres, K.S. Novoselov, A.K. Geim, *Rev. Mod. Phys.* **81**, 109 (2009)
3. J.M.B. Lopes dos Santos, N.M.R. Peres, A.H. Castro Neto, *Phys. Rev. Lett.* **99**, 256802 (2007)
4. J.M.B. Lopes dos Santos, N.M.R. Peres, A.H. Castro Neto, *Phys. Rev. B* **86**, 155449 (2012)
5. S. Shallcross, S. Sharma, E. Kandelaki, O.A. Pankratov, *Phys. Rev. B* **81**, 165105 (2010)
6. R. Bistritzer, A.H. MacDonald, *Phys. Rev. B* **81**, 245412 (2010)
7. E.J. Mele, *Phys. Rev. B* **81**, 161405(R) (2010)
8. R. Bistritzer, A.H. MacDonald, *Proc. Natl. Acad. Sci.* **108**, 12233 (2011)
9. G. Trambly de Laissardière, D. Mayou, L. Magaud, *Nano Lett.* **10**, 804 (2010)
10. E.V. Castro, K.S. Novoselov, S.V. Morozov, N.M.R. Peres, J.M.B. Lopes dos Santos, J. Nilsson, F. Guinea, A.K. Geim, A.H. Castro Neto, *J. Phys.: Condens. Matter* **22**, 175503 (2010)
11. M. Kindermann, E.J. Mele, *Phys. Rev. B* **84**, 161406(R) (2011)
12. L. Meng, Z.-D. Chu, Y. Zhang, J.-Y. Yang, R.-F. Dou, J.-C. Nie, L. He, *Phys. Rev. B* **85**, 235453 (2012)
13. T. Ohta, J.T. Robinson, P.J. Feibelman, A. Bostwick, E. Rotenberg, T.E. Beechem, *Phys. Rev. Lett.* **109**, 186807 (2012)
14. C.J. Tabert, E.J. Nicol, *Phys. Rev. B* **87**, 121402(R) (2013)
15. Z.-D. Chu, W.-Y. He, L. He, *Phys. Rev. B* **87**, 155419 (2013)
16. W. Landgraf, S. Shallcross, K. Türschmann, D. Weckbecker, O. Pankratov, *Phys. Rev. B* **87**, 075433 (2013)
17. X. Zou, J. Shang, J. Leaw, Z. Luo, L. Luo, C. La-o-vorakiat, L. Cheng, S.A. Cheong, H. Su, J.-X. Zhu, Y. Liu, K. Ping Loh, A.H. Castro Neto, T. Yu, E.E.M. Chia, *Phys. Rev. Lett.* **110**, 067401 (2013)
18. M. Mecklenburg, B.C. Regan, *Phys. Rev. Lett.* **106**, 11680 (2011)
19. G. Tkachov, *Phys. Rev. B* **79**, 045429 (2009)

20. M.I. Katsnelson, K.S. Novoselov, *Solid State Commun.* **143**, 3 (2007)
21. F. de Juan, A.G. Grushin, M.A.H. Vozmediano, *Phys. Rev. B* **82**, 125409 (2010)
22. M.I. Katsnelson, K.S. Novoselov, A.K. Geim, *Nat. Phys.* **2**, 620 (2006)
23. F.D.M. Haldane, *Phys. Rev. Lett.* **61**, 2015 (1988)
24. G.W. Semenoff, *Phys. Rev. Lett.* **53**, 2449 (1984)
25. S.Y. Zhou, D.A. Siegel, A.V. Fedorov, F. El Gabaly, A.K. Schmid, A.H. Castro Neto, A. Lanzara, *Nat. Mater.* **7**, 259 (2008)
26. S.Y. Zhou, G.H. Gweon, A.V. Federov, P.N. First, W.A. De Heer, D.H. Lee, F. Guinea, A.H.C. Neto, A. Lanzara, *Nat. Mater.* **6**, 770 (2007)
27. A.L. Walter, S. Nie, A. Bostwick, K.S. Kim, L. Moreschini, Y.J. Chang, D. Innocenti, K. Horn, K.F. McCarty, E. Rotenberg, *Phys. Rev. B* **84**, 195443 (2011)
28. N. Kharche, S.K. Nayak, *Nano Lett.* **11**, 5274 (2011)
29. R. Dillenschneider, J.H. Han, *Phys. Rev. B* **78**, 045401 (2008)
30. I. Santos, P.K. Gogoi, H.B. Su, H. Huang, Y. Lu, D. Qi, W. Chen, M.A. Majidi, Y.P. Feng, A.T.S. Wee, K.P. Loh, T. Venkatesan, R.P. Saichu, A. Goos, A. Kotlov, M. Rübhausen, A. Rusydi, *Phys. Rev. B* **84**, 081403 (R) (2011)
31. A. Bostwick, T. Ohta, T. Seyller, K. Horn, E. Rotenberg, *Nat. Phys.* **3**, 36 (2007)
32. N.M.R. Peres, R.M. Ribeiro, A.H. Castro Neto, *Phys. Rev. Lett.* **105**, 055501 (2010)
33. L. Yang, *Phys. Rev. B* **83**, 085405 (2011)
34. F. Fallah, M. Esmailzadeh, *J. Appl. Phys.* **114**, 073702 (2013)
35. D. Xiao, W. Yao, Q. Niu, *Phys. Rev. Lett.* **99**, 236809 (2007)
36. G. Giovannetti, P.A. Khomyakov, G. Brocks, V.M. Karpan, J. van den Brink, P.J. Kelly, *Phys. Rev. Lett.* **101**, 026803 (2008)
37. S.Y. Shin, N.D. Kim, J.G. Kim, K.S. Kim, D.Y. Noh, K.S. Kim, J.W. Chung, *Appl. Phys. Lett.* **99**, 082110 (2011)
38. J. Chen, M. Badioli, P. Alonso-Gonzalez, S. Thongrattanasiri, F. Huth, J. Osmond, M. Spasenovic, A. Centeno, A. Pesquera, P. Godignon, A. Zurutuza Elorza, N. Camara, F.J. Garcia de Abajo, R. Hillenbrand, F.H.L. Koppens, *Nature* **487**, 77 (2012)
39. Z. Fei, A.S. Rodin, G.O. Andreev, W. Bao, A.S. McLeod, M. Wagner, L.M. Zhang, Z. Zhao, M. Thiemens, G. Dominguez, M.M. Fogler, A.H. Castro Neto, C.N. Lau, F. Keilmann, D.N. Basov, *Nature* **487**, 82 (2012)
40. O.F. Dayi, A. Jellal, *J. Math. Phys.* **51**, 063522 (2010)
41. C. Bastos, O. Bertolami, N.C. Dias, J.N. Prata, *Int. J. Mod. Phys. A* **28**, 1350064 (2013)
42. V.A. Rubakov, M.E. Shaposhnikov, *Phys. Lett. B* **125**, 136 (1983)
43. A. Lukas, B.A. Ovrut, K.S. Stelle, D. Waldram, *Phys. Rev. D* **59**, 086001 (1999)
44. R. Davies, D.P. George, R.R. Volkas, *Phys. Rev. D* **77**, 124038 (2008)
45. Y.-X. Liu, L.-D. Zhang, L.-J. Zhang, Y.-S. Duan, *Phys. Rev. D* **78**, 065025 (2008)
46. M. Sarrazin, F. Petit, *Phys. Rev. D* **81**, 035014 (2010)
47. F. Petit, M. Sarrazin, *Phys. Lett. B* **612**, 105 (2005)
48. M. Sarrazin, F. Petit, *Int. J. Mod. Phys. A* **22**, 2629 (2007)
49. M. Sarrazin, G. Pignol, F. Petit, V.V. Nesvizhevsky, *Phys. Lett. B* **712**, 213 (2012)
50. A. Connes, J. Lott, *Nucl. Phys. B* **18**, 29 (1991)
51. A. Connes, *Non-Commutative Geometry* (Academic Press, San Diego, 1994)
52. N.A. Viet, K.C. Wali, *Phys. Rev. D* **67**, 124029 (2003)
53. N.A. Viet, K.C. Wali, *Int. J. Mod. Phys. A* **11**, 533 (1996)
54. L.P. Colatto, A.L.A. Penna, W.C. Santos, *Phys. Rev. D* **73**, 105007 (2006)
55. O. Bertolami, R. Queiroz, *Phys. Lett. A* **375**, 4116 (2011)
56. H. Falomir, J. Gamboa, M. Loewe, F. Méndez, J.C. Rojas, *Phys. Rev. D* **85**, 025009 (2012)
57. L.C. Smith, J.J. Davies, D. Wolverson, H. Boukari, H. Mariette, V.P. Kochereshko, R.T. Phillips, *Phys. Rev. B* **83**, 155206 (2011)
58. J.J. Davies, D. Wolverson, V.P. Kochereshko, A.V. Platonov, A.F. Ioffe, R.T. Cox, J. Cibert, H. Mariette, C. Bodin, C. Gourgon, E.V. Ubyivovk, Yu.P. Efimov, S.A. Eliseev, *Phys. Rev. Lett.* **97**, 187403 (2006)
59. A. Tonomura, T. Matsuda, B. Suzuki, A. Fukuhara, N. Osakabe, H. Umezaki, J. Endo, K. Shinagawa, Y. Sugita, H. Fujiwara, *Phys. Rev. Lett.* **48**, 1443 (1982)
60. A. Tonomura, H. Umezaki, T. Matsuda, N. Osakabe, J. Endo, Y. Sugita, *Phys. Rev. Lett.* **51**, 331 (1983)
61. H. Doll, M. Nábauer, *Phys. Rev. Lett.* **7**, 51 (1961)
62. V. Perebeinos, J. Tersoff, P. Avouris, *Nano Lett.* **5**, 2495 (2005)
63. C.D. Spataru, S. Ismail-Beigi, R.B. Capaz, S.G. Louie, *Phys. Rev. Lett.* **95**, 247402 (2005)
64. S. Albrecht, S. Schäfer, I. Lange, S. Yilmaz, I. Dumsch, S. Allard, U. Scherf, A. Hertwig, D. Neher, *Org. Electron.* **13**, 615622 (2012)
65. V.I. Klimov, *J. Phys. Chem. B* **110**, 16827 (2006)